https://dx.doi.org/10.22161/ijaers.6.2.24 *ISSN: 2349-6495(P) | 2456-1908(O)*

Thin Film of Nickel-Zinc Solar Absorber Deposited on Nanostructured Copper Substrate by Reactive Electron-Beam Evaporation

Ricardo Luiz Perez Teixeira[1], José Carlos de Lacerda[2]

[1] Materials Engineering Course, Institute of Integrated Engineering, Federal University of Itajuba, Itabira-MG, Brazil
Email: ricardo.luiz@unifei.edu.br
[2] Mechanical Engineering Course, Institute of Integrated Engineering, Federal University of Itajuba, Itabira-MG, Brazil

***Abstract*—** *This article deals with the motivation for development of selective thin film on structured substrate in the field of upgrading solar energy conversion. Some observations on reactive PVD E-beam and structural and optical properties of nickel-zinc solar absorber obtained were briefly discussed. The thin film of nickel-zinc obtained shows optimum optical properties as far as maximum absorptance and minimum emittance, these results verified closed to the Planck black body and the ideal selective film. The nickel-zinc oxides from the thin film obtained allow exceptional stability and semiconductor properties, make practical applications feasible for future photovoltaics designs.*

Keywords*— *Nanostructuration, Nickel-zinc thin film, Reactive PVD E-beam, Solar absorber surface, Sol-gel antireflection layer of SiO_2.

I. INTRODUCTION

The flat plate collectors are based on two important principles: a black base that absorbs the solar radiation better than any other color and a glass lid that is needed to keep the heat in[1,2]. An ideal solar selective (solar absorber) coating must have then high solar absorptance and low emittance [3,4]. Several techniques, such as vacuum techniques (sputtering, electron beam, chemical vapor deposition, etc.), sol-gel, electrochemical and electroless deposition (catalytic reduction process) are currently used to produce solar absorber surfaces, but two types are mainly applied in industry: vacuum and electrochemical techniques [5]. In this work, black nickel-zinc solar absorber layers are deposited on copper C81100 substrates by REACTIVE electron-beam evaporation (PVD E-beam). After nickel-zinc thin film deposition a sol-gel antireflection coating of SiO_2 is applied to each solar absorber surface obtained by the spin coating method. The thicknesses of the layers have to be nanostructured in order to avoid absorption by interference for wavelengths in the middle of the solar spectrum (solar light trapping effects), the substrate nanostructuration. The characteristics of the nickel-zinc absorber film revealed by atomic force microscopy (AFM), X-ray diffraction (XRD) and optical UV-VIS-NIR and MIR spectrophotometry (optical proprieties) shows beneficial effects of the nanostructuration proposed and PVD E-beam technique on their optical characteristics.

II. EXPERIMENTAL PROCEDURE

The proposed nickel-zinc thin film on nanostructured were obtained using the following sequence of operations:

1) Nanometric leveling of metallic substrates: mechanical unidirectional polishing (P1200) of C81100 copper substrates (1 × 1 cm^2); copper electrochemical polishing (electropolished) in 85 %v/v H_3PO_4 a 1750 mV (DC) for 180 seconds (3 × 60 seconds), only for nanostructured sample [6];

2) Deposition of the solar absorber coating:

Reactive PVD E-beam[9]: nickel and ZnO powder particles are used as source materials to deposition by PVD electron beam evaporation, O_2 introduced into the chamber (working pressure: 1.3×10^{-3} Pa). The electron gun voltage applied were of 4kV to7kV and working current were of 300 to 500 mA for 15 minutes. Target composition equivalent to the electrochemical condition or procedure: 3Ni:ZnO [8]. The E-beam solar absorber surface presented a Filmetrics™ F20 estimated thickness of about 1-2 μm on nanometric leveled C81100 copper substrate.

3) Sol-gel antireflection layer of SiO_2 [10]: the antireflection coating, from tetraethylorthosilicate (TEOS), was made by the spin coating method. The antireflection coating of SiO_2 presented a DekTak™ IIA profilometer estimated thickness of 200 nm.

All chemical reactants and solutions were made from Vetec chemicals (Vetec Química Fina Ltda) and Milli-Q™ water.

4) Scanning Electron Microscopy (SEM) and Energy Dispersive X-ray (EDS) spectroscopy of the absorber samples were performed using JEOL JSM-6460 LV and EDX Noran in 200 kV (EDS), respectively. Back scattered

https://dx.doi.org/10.22161/ijaers.6.2.24 *ISSN: 2349-6495(P) | 2456-1908(O)*

electron imaging, qualitative X-ray analysis, and cross-section images were obtained.

Ultraviolet-visible- near infrared spectroscopy (UV-VIS-NIR absorption patterns) of the absorber samples were obtained using a Perkin Elmer™ Lambda 950 spectrophotometer with wavelength of 175 nm at 2500 nm, Labsphere's Spectralon® reflectance material was used as standard sample for calibration (reflectance > 95%). FTIR spectra and mid infrared emittance results (MIR or thermal infrared, wavelength of 3 μm to 8 μm) of the absorber surface were analyzed with Perkin Elmer Spectrum GX using as reference a polished nickel plate (with reflectance > 95 %) with wavelength of 2500 nm at 7000 nm.

The thin film thicknesses were evaluated using Filmetrics™ F20 also. To determine film thickness, the Filmetrics™ F20 software calculates a reflectance spectrum that matches as closely as possible to the measured spectrum, the thickness baseline. To determine the anti-reflective layer thickness were only used a DekTak™ IIA profilometer.

AFM images of the absorber samples were recorded using intermittent contact mode operation on a JPK™ atomic force microscope (JPK Instruments- Nanotechnology for Life Science) under ambient condition, relative humidity between 45% and 55%. Micromasch™ rectangular cantilever NSC16/AlBS has been employed to obtain topography and phase contrast images. Magnetic force microscopy (MFM) images of the absorber surface were obtained by using the same tips coated with Co-Cr. Image resolution has been set to 512×512 points.

X-ray diffraction patterns were obtained using a Rigaku MiniFlex™ X-ray Diffraction System adapted to measure non-powder XRD on Back Filled Holder. The goniometer of radiation operating at 30 keV and 15 mA (Cu Kα) with nickel filter produces monochromatic X-rays focused on the sample surface to determine by Bragg Law the interplanar spacing (d-spacing). The analysis range of 2×theta was between 10° and 100° with a 0.05° step. The data was analyzed by XRD analysis software Jade™ (Jade 5.0.37 from Materials Data, Inc).

III. RESULTS AND DISCUSSION

3.1 Optical Analysis – Spectrometry UV, VIS, nIR and mIR

The normal reflectance of prepared samples was measured in the wavelength interval (λ) 0.3 to 2.50 μm by a Perkin-Elmer Lambda 950 spectrophotometer with an integrating sphere. The solar absorptance (α in equation 1) is theoretically defined as a weighted fraction between absorbed radiation and incoming solar radiation. The direct normal solar irradiance (I_{sol}) is defined according to the ISO standard 9845-1 (1992) where an air mass of 1.5 (ASTM E891-1987) is used. Normal thermal emittance (ε in equation 2) is a weighted fraction between emitted radiation and the Planck black body distribution (I_p, equation 4: σ is Stefan Boltzmann constant, 5.67 ×10^{-8} W m^{-2} K^{-4} and T_o is the absolute temperature of heated surface at steady-state) at 100ºC (373 K). Selectivity is the comparative fraction between absorptance and emittance. The ideal selective surface in Figure 1 has zero reflectance (R, □ = 1 – R = 1 or 100 %) to λ between 0.3 and 2.5 □m and unity reflectance (R, □ = 1 –R = 0 or 0 %) in the infrared region, to λ between 2.5 and 25 □m [2,11]. The antireflection sol-gel coating of SiO_2 presented an emittance of about 5 % (smooth glass)[2,10].

$$\alpha_{sol} = \frac{\int_{0.3\mu m}^{2.5\mu m} (1 - R(\lambda)) \cdot I_{sol}(\lambda) \cdot d\lambda}{\int_{0.3\mu m}^{2.5\mu m} I_{sol}(\lambda) \cdot d\lambda} \quad (1)[11]$$

$$\varepsilon_{therm} = \frac{\int_{2.5\mu m}^{20\mu m} (1 - R(\lambda)) \cdot I_p(\lambda) \cdot d\lambda}{\int_{2.5\mu m}^{20\mu m} I_p(\lambda) \cdot d\lambda} \quad (2)[11]$$

$$\varepsilon_\lambda + R_\lambda = \alpha_\lambda + R_\lambda = 1 \quad (3)[11]$$

$$I_p \approx \sigma \cdot \left(T_o^4\right) \quad (4)\ [11]$$

In Figure 1 and 2, the absorptance for both structuration conditions for □ = 300 - 2500 nm shows a statistical optical improvement in α with E-beam with absorptance (99,6 ± 0.1) % of the E-beam condition. The results of solar absorptance indicate that the optical parameters of the absorber samples are improved by the deposition technique and nanostructuration of substrate. The emittance for both structuration conditions for □ = 2500 nm to 25000 nm shows a decreasing s in ε with reactive PVD E-beam, thus the emittance of 8.4 % of the electrochemical condition and 10.4 % or □ = 2500 nm to 25000 nm. The thin film deposited presented a highly selectivity (solar absorptance and thermal/ emittance) value of 11.55 (0.9703/0.084 due a nickel-zinc electrochemical solar absorber on nanostructured copper substrates). This result of selectivity was improved using an antireflection SiO_2 sol-gel coating with emittance values of 0.05 [2,10]. The PVD E-beam film measured by the Filmetrics™ F20 shows a thin film with a thickness from 1μm to 2 μm. Table 1 shows that the thin film behave are close to an ideal selective material, with the absorptance close to Plank black body.

https://dx.doi.org/10.22161/ijaers.6.2.24 *ISSN: 2349-6495(P) | 2456-1908(O)*

Table.1. Mid-temperature of some black selective surfaces[2].

Material	Fabrication Method	α	ε (100 °C)	Product
Black nickel NiS-ZnS	Electrodeposition	0.98 - 0.96	0.03 - 0.10	Maxorb
Black copper BlCu-Cu_2O:Cu	Electrodeposition / Sol-gel	0.97 - 0.98	0.02	
Black chrome Cr-Cr_2O_3	Electrodeposition	0.97	0.09	MTI Chrome Coat Energie Solaire
Ni-NiO_x	Reactive sputtering	0.96	0.10	Sunstrip
Ni pigmented Al_2O_3	Anodization	0.85 - 0.97	0.08 - 0.21	TeknoTerm Energi Showa

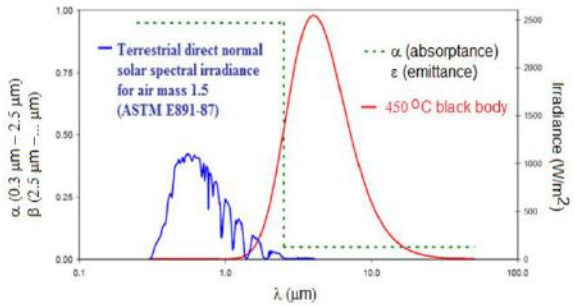

Fig.1: Spectral performance of an ideal selective solar absorber[2].

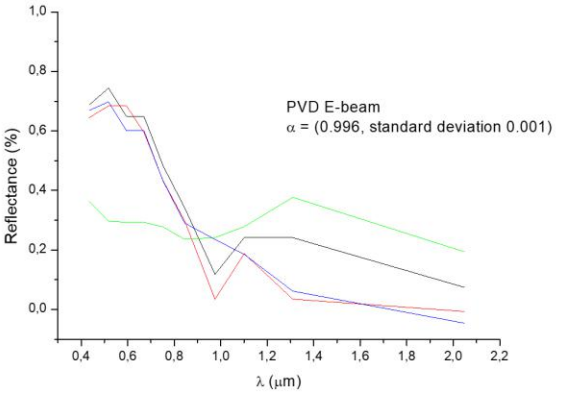

Fig.2: Solar reflectance (λ = 350 nm-2000 nm, 450 K) of thin film with an antireflection sol-gel layer of SiO_2.

3.2 Topography and Physical Analysis: Atomic Force Microscopy

AFM micrometric image of samples - Figure 3(a) and Figure 3(b) - compare the P1200 polished and electropolished samples and show the nanometric leveling effects on the surface of the electropolished copper plates via a multistep method. The JPK™ root mean square roughness (RMS) deviation has decreased from 114.6 nm (submicrometric) in the mechanical polished surface to 24.5 nm in the electropolished surface. Also, the JPK™ maximum peak height is reduced from (504.1± 0.1) nm (mechanical polished surface) to (39.8 ± 0.1) nm (electropolished surface). Furthermore, a better height distribution in the electropolished copper surface was registered. Thus, JPK™ AFM analysis results show that copper bulk is nanometrically leveled.

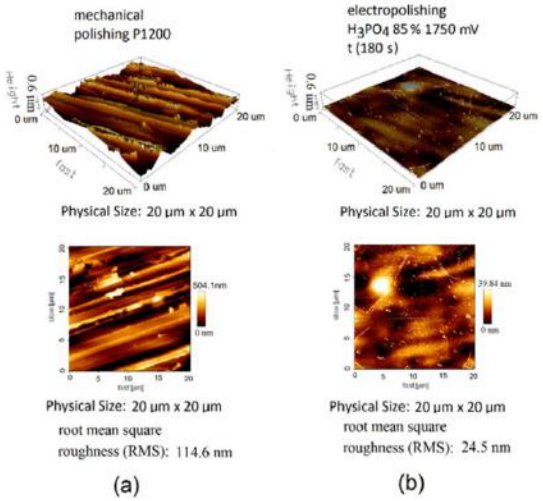

Fig.3: AFM 20 µm × 20 µm images and statistical JPK™ roughness of the surface nanometric leveling of (a) copper mechanical P1200 polished with and (b) copper electropolished at 1750 mV (DC), in H_3PO_4 85 %v/v for 180 s [6].

To confirm the dimensions of the nickel-zinc solar absorber surfaces to both conditions, phase contrast and topography scanning images were performed with SPIP™ image analyses. In Figure 4, AFM SPIP™ parameters of the nickel-zinc thin film indicate the presence of smaller and some periodic nanometric grains with an estimate mode particle size of 20 nm, an average and a maximum height roughness of 71 fm and 21.1 nm (respectively), besides, the thin film presented an AFM JPK™ a roughness deviation of 2.7 nm. AFM JPK™ RMS and maximum height roughness for the thin film is lower than sunlight wavelengths and therefore, the surface texturing or trapping effects related by Kennedy; this consideration means that sunlight absorbing effect is improved using PVD E-beam technique [3].

https://dx.doi.org/10.22161/ijaers.6.2.24 *ISSN: 2349-6495(P) | 2456-1908(O)*

Fig.4: AFM of thin film. (a) 4 ×4 μm images of the height (topography profile) and (b) 4 ×4 μm lock-in phase image.

3.3. Morphology: Scanning Electron Microscopy (SEM) and Energy Dispersive X-ray (EDS) spectroscopy

Images of SEM (and EDS), Figure 5 (a) show a smooth and continuous surface for the thin film. Analysis of EDS for the electrochemical condition, Figure 5(b) showed the presence of zinc and nickel for the thin film. The nickel/zinc percentage atomic composition EDS rate found for the electrochemical condition is 80%/20 % in the PVD E-beam deposition.

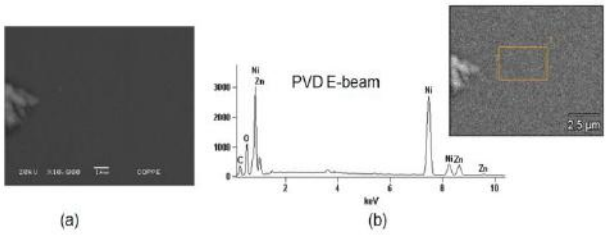

Fig.5: (a) SEM 10,000× image and (b) EDS spectrum of thin film.

3.4. Chemical Analysis: Fourier Transform Infrared (FTIR)

FTIR literature broad bands in table 2 were used to study the chemical composition of the absorber film type nickel-zinc using to the electrochemical and E-beam conditions.

The infrared spectrum of the PVD E-beam condition in Figure 8 exhibits broad bands, centered at zinc oxide and nickel oxide, this result agree with EDS (Figure 7(b)) also. The FTIR results in Figure 6 showed nickel and zinc oxides with indicatives close to Dharmaraj and Ghule for the NiO and ZnO nanoparticles FTIR broad bands [13,16]. The presence of thiocyanate and indicatives of ZnS were detected only in the electrochemical condition. Therefore, were basically produced a black zinc-nickel absorber surfaces by electrochemical and evaporation (PVD E-beam) methods with a chemical composition of zinc and nickel oxides. The results obtained from FTIR are equivalents with those obtained previously by XPS [6,8].

Table 2. FTIR absorption bands of thin film.

Identification	Absorption, broad bands	Intensity (%)
NiO[12]	600-680 cm^{-1}	3
	830-930 cm^{-1}	70
	1000-1130 cm^{-1}	10
NiO[13, 14, 15]	420-440 cm^{-1}, 475-480 cm^{-1}, 445-490 cm^{-1}, 1633 cm^{-1} e 3470 cm^{-1}	-
Zn (2+)[16]	870-900 cm^{-1} e 1047-1050 cm^{-1}	-
ZnO[17,18]	450-460 cm^{-1}, 1486 cm^{-1}, 1600-1630 cm^{-1} e 3410-3420 cm^{-1}	-

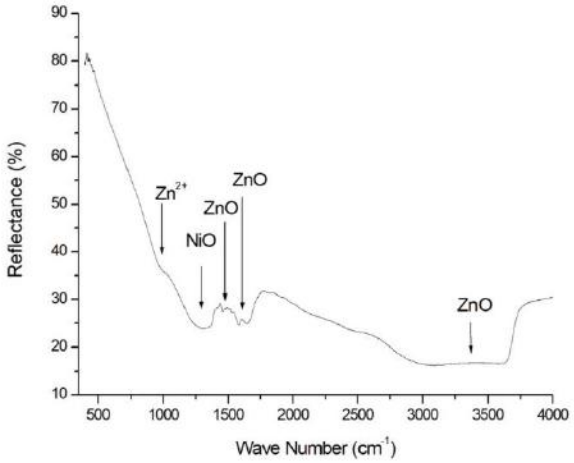

Fig.6: FTIR of thin film.

3.5. X-ray diffraction (XRD)

Figure 7 shows the XRD pattern for ZnO and NiO of thin film on copper substrate. XRD to detect some peaks of NiO (200), NiO(220), ZnO (200) and other Lattice planes NiO beyond copper substrate signals. The peak at about 45° and 43° corresponds to the diffraction from (002) plane of ZnO e (200) NiO, indicating an oriented ZnO and NiO growth along the c-axis perpendicular to the substrate surface [22, 23, 24]. The results obtained from XRD are consistent with those obtained previously by XPS [6,8].

https://dx.doi.org/10.22161/ijaers.6.2.24 *ISSN: 2349-6495(P) | 2456-1908(O)*

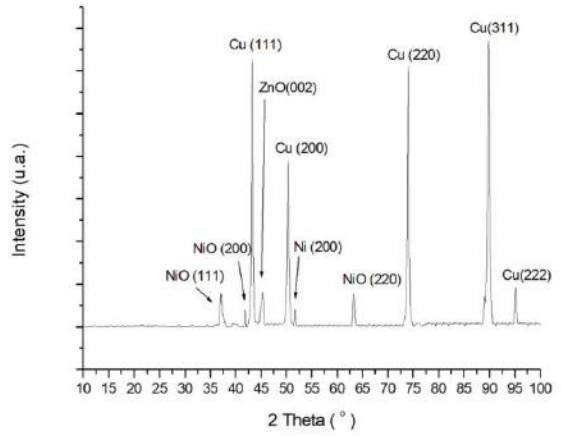

Fig.7: XRD pattern NiO-ZnO of thin film.

IV. CONCLUSIONS

The results of solar absorptance and selectivity indicate that the optical parameters of the absorber samples were improved by the PVD E-beam deposition technique and nanostructuration of substrate when compared with commercial optical selective films. The thin film of nickel-zinc oxide deposited offered a highly selectivity of 11.55 (0.9703/0.084) close to the ideal optical selective film and absorptance close to the Planck black body.

AFM images confirmed the success of the surface nanostructuration of the copper bulk RMS roughness and thin film. The results of solar absorptance indicate that the optical parameters of the absorber samples are improved by nanostructuration of the copper substrate.

The FTIR and XRD results showed a ZnO semiconductor thin film PVD E-beam were deposited on copper substrate making this thin film feasible for future photovoltaics designs in solar power plants.

V. ACKNOWLEDGEMENTS

Thanks to UNIFEI Campus Itabira, The GPESE UNIFEI Research Group, The LIMAV UNIFEI Research Group, PEMM-COPPE-UFRJ and Professor Renata Antoun Simão for support in the experiments.

REFERENCES

[1] Hae-Sung, Y., Eun-Seob, K., Min-Soo, K., Jang-Yeob, L., Gyu-Bong, L., Sung-Hoon, A. (2015). Towards greener machine tools – A review on energy saving strategies and technologies. Renewable and Sustainable Energy Reviews, 48, 870-891.

[2] Yadav D., Banerjee R. (2016). A review of solar thermochemical processes. Renewable and Sustainable Energy Reviews, 54, 497-532.

[3] Kennedy C. E. (2002). Review of Mid- to High-Temperature Solar Selective Absorber Materials. NREL National Renewable Energy Laboratory.

[4] Keith, S., Andrew, W., Mengya, L., Cary, L. P. (2016) Surface engineering of nanomaterials for improved energy storage – A review. Chemical Engineering Science; 154 (2), 3-19.

[5] Zhang, K., Hao, L., Du, M., Mi, J., Wang, J., Meng, J. (2017). A review on thermal stability and high temperature induced ageing mechanisms of solar absorber coatings. Renewable and Sustainable Energy Reviews, 67, 1282-1299.

[6] Teixeira R. L. P., Simão R. A., Coelho, B., Oliveira, A. C. (2011). Nanometric leveling and optical selectivity enhancement of black nickel electrodeposited on C81100 high conductive copper. International Journal of Energy and Environment , 2 (5), 266-273.

[7] Dennis, J. K., Such, T. E. (1972). Nickel chromium plating, Butterworth & Co.(Publishers) Ltda, London; Ch. 4 and 5.

[8] Teixeira, R. L. P., Raniero, L., Simão, R. A., Coelho, B, Oliveira, A.C. (2011). Temperature influence on the thermal and structural properties of electrodeposited nanostructured black nickel's cermet on high conductive C81100 copper. Int. J. Low-Carbon Tech. Low Carbon,. 6, 86-92.

[9] Xu, L., Shi, L., Li, X. (2008). Effect of TiO2 buffer layer on the structural and optical properties of ZnO thin films deposited by E-beam evaporation and sol-gel method. Appl. Surf. Sc, 255, 3230-3234.

[10] Morales, A., Bautista, M. C., Cáceres, D. (2004). Recubrimientos antirreflectantes de sílice sobre vidrio producidos por sol-gel. Bol. Soc. Esp. Ceram., 43, 455-456.

[11] Boström, T., Wäckelgård, E., Westin, G. (2003). Solution-chemical derived nickel-alumina coatings for thermal solar absorbers. Solar Energy, 74, 497-503.

[12] Spectrum. (2005). PerkimElmer's Data Sheet Spectrum v5.3.1.

[13] Sade, W., Nunes, R. A. X., Branco, J. R. T. (2009). Deposição Química de Filmes de Ni/NiO em Substrato de Alumínio. Metalurgia & Materiais. REM: R. Esc. Minas, Ouro Preto, 62(3), 361-365.

[14] Dharmaraj, N., Prabu, P., Nagarajand, S., Kim, C. H., Park, J. H., Kim, H. Y. (2006). Synthesis of nickel oxide nanoparticles using nickel acetate and poly (vinyl acetate) precursor. Materials Science and Engineering B, 128(1-3), 111-114.

[15] Biju, V., Abdul Khadar, M. (2003). Fourier transform infrared spectroscopy study of nanostructured nickel oxide. Spectrochimica Acta, Part A, 59, 121-134.

[16] Sun, X., Wang, S., Liu, X., Gong, W., Bao, N., Gao, B. (2008). Competitive biosorption of zinc(II) and cobalt(II) in single- and binary-metal systems by

https://dx.doi.org/10.22161/ijaers.6.2.24 *ISSN: 2349-6495(P) | 2456-1908(O)*

aerobic granules. Journal of Colloid and Interface Science, 324, 1-8.

[17] Ghule, K., Ghule, A. V., Chen, B., Ling, Y. (2006). Preparation and characterization of ZnO nanoparticles coated paper and its antibacterial activity study. Green Chem, 8, 1034-1041.

[18] Bhattacharya, R. N., Ramanathan, K., Gedvilas, L., Keyes, B. (2005). Cu(In,Ga)Se2 thin-film solar cells with ZnS(O,OH), Zn–Cd–S(O,OH) and CdS buffer layers. Journal of Physics and Chemistry of Solids, 66: 1862-1864.

[19] Arvind, A., Agrawal, S. L. (2007). Structural, thermal and electrical characterizations of PVA:DMSO:NH4SCN gel electrolytes. Solid State Ionics, 178 (13-14): 951-958.

[20] Ramya, C. S., Selvasekarapandian, S., Hirankumar, G., Savitha, T., Angelo, P. C. (2008). Investigation on dielectric relaxations of PVP–NH4SCN polymer electrolyte. Journal of Non-Crystalline Solids, 358: 1494-1502.

[21] Dreesen, L., Volcke, C., Sartenaer, Y., Peremans, A., Thiry, P. A., Humbert, C., Grugier, J., Marchand-Brynaert, J. (2006). Comparative study of decyl thiocyanate and decanethiol self-assembled monolayers on gold substrates. Surface Science, 600 (18), 4052-4057.

[22] Papadimitriou, D. N. (2016). Structural, optical, electrical properties, and strain/stress of electrochemically deposited highly doped ZnO layers and nanostructured ZnO antireflective coatings for cost-effective photovoltaic device technology. Thin Solid Films, 605 (30), 215-231.

[23] Alshahrie, A., Yahia, I. S., Atteiah Alghamdi, Al Hassan, P. S. (2016) Morphological, structural and optical dispersion parameters of Cd-doped NiO nanostructure thin film. Optik - International Journal for Light and Electron Optics, 127 (12), 5105-5109.

[24] Moon, J., Jong-Sook. L., Park, J., Su-Jae, L., Zyung, T. (2010). Two-dimensional ZnO–NiO macroporous arrays: Fabrication, structure and electrical properties. Electrochimica Acta, 55 (22), 6849-6856.